Journal of Non-Crystalline Solids 371–372 (2013) 28–32

Contents lists available at SciVerse ScienceDirect

Journal of Non-Crystalline Solids

journal homepage: www.elsevier.com/ locate/ jnoncrysol

# Microstructures, phases, and properties of low melting $BaO–B_2O_3–ZnO$ glass films prepared by pulsed laser deposition

Ruqiang Bao *, Carl M. Busta, Xiaofeng Su, Minoru Tomozawa, Douglas B. Chrisey [1]

*Department of Materials Science and Engineering, Rensselaer Polytechnic Institute, Troy, NY 12180 USA*

ARTICLE INFO

*Article history:*
Received 24 January 2013
Received in revised form 28 March 2013
Available online 10 May 2013

*Keywords:*
Low melting glass;
Viscous flow liquid phase sintering;
High performance capacitor;
Pulsed laser deposition;
Microstructural evolution

ABSTRACT

With the motivation to employ $BaO–B_2O_3–ZnO$ for high performance capacitors by using viscous flow/liquid phase sintering, the microstructures, phases, and dielectric properties of $BaO–B_2O_3–ZnO$ films prepared by pulsed laser deposition were examined as a function of heat-treatment. The glass transition temperature ($T_g$) and crystallization temperature of the films are ~536 °C and 640 °C, respectively. The phases in the films are quite complicated after heat-treated above 700 °C until 900 °C where the film is dominated by a single phase. Zn concentration is reduced after heat-treatment at high temperature due to segregation and evaporation. The dielectric constant of the film decreases with the increasing heat-treatment temperature, probably due to Zn reduction, Si diffusion, and crystallization of the film. Experimental data shows that ~700 °C is the optimal temperature to use the low melting glass $BaO–B_2O_3–ZnO$ to make high performance capacitors by viscous flow/liquid phase sintering.



## 1. Introduction

One of the great challenges for incorporating renewable energy sources in the 21st century is energy storage [1]. In order to meet the challenge of global warming and the limited supply of fossil fuels, new energy technologies are being developed to harvest environmentally friendly and renewable energy sources, e.g., solar photovoltaic, wind, and tidal sources. Limited energy storage capacity [2] is becoming a key bottleneck to large-scale power generation from such energy sources, which face geographical restrictions and variable output [3]. The current approaches to large-scale energy storage include compressed air and pumped hydroelectric which are similarly, geographically restricted and new approaches are needed. Capacitive energy storage is a novel approach for large-scale energy storage. The amount of electrostatic energy that can be stored in capacitors is limited by the permittivity and breakdown strength of the materials used. Therefore, breakthroughs and innovations in materials play the key role in enhancing the new generations of energy storage using a capacitive approach.

A low melting glass with high dielectric constant is critical for high energy density capacitors. Multilayer ceramic capacitor (MLCC) is the dominant approach to ceramic capacitor fabrication because of its very high volumetric/gravimetric storage density resulting from the combination of large electrode area, thin dielectric layers, high dielectric breakdown strength, and high permittivity dielectrics [4]. The foremost issue in MLCC fabrication is the processing temperature mismatch, since the ceramic dielectric sintering temperature (>1200 °C) is higher than the melting temperature of many electrode materials. The employment of high temperature sintering processes gives rise to many challenges like the diffusion of electrode material into the dielectric, which in turn has a strong influence on the leakage current density, the capacitance, the breakdown voltage, and the time-dependent dielectric breakdown. Therefore, low melting temperature glassy components can help reduce the sintering temperature of high-k dielectrics such as $BaTiO_3$ ($\kappa$ ~ 2500 [5]) with the sintering temperature of ~1400 °C [6]. Low melting temperature glass can mitigate the porosity and diffusion of electrode material into the dielectric stack. As a consequence, dielectric breakdown strength [7], energy density [8,9] and the time-dependent dielectric breakdown can be improved. In addition, the low temperature process can reduce the agglomeration of nano-particles and thus maintain the unique properties of nano-particles. The dielectric properties of $BaTiO_3$-based (PbO-free) materials are highly dependent on grain size [10], especially in the submicron size range. Research shows that the room temperature dielectric constant of $BaTiO_3$ is about 5000 for pure nano-size fine powders (~40 nm), while that of micro-size coarse powders (~2 mm) is only about 2200 [11]. Processes such as viscous flow/liquid phase sintering can be employed to lower the sintering temperature for nano-sized ceramic powder and help reduce the coarsening of nano-particles to improve the capacitor performance.

Low melting glasses usually can be achieved in PbO-based glass system with the glass transition temperature ($T_g$) from 520 to 650 °C [12,13] or in Pb-free but $Bi_2O_3$-based system such as $Bi_2O_3–$

* Corresponding author at: IBM Semiconductor Research and Development Center, Hopewell Junction, NY 12533, USA. Tel.: +1 845 894 5698.
*E-mail address:* rbao@us.ibm.com (R. Bao).
[1] Currently at Department of Physics and Engineering Physics, Tulane University, New Orleans, LA 70118, USA.

0022-3093/$ – see front matter © 2013 Elsevier B.V. All rights reserved.
http://dx.doi.org/10.1016/j.jnoncrysol.2013.04.005

$B_2O_3$–ZnO–BaO–$A1_2O_3$ ($T_g$ = 480–500 °C) [14]. But there are a number of problems associated with their use. In PbO-based system, Pb is deleterious to the health and the environment. In the case of $Bi_2O_3$-based system, bismuth is expensive because of its scarcity. Fortunately, Pb-free BaO–$B_2O_3$–ZnO glass has low-melting characteristics and has been considered as a candidate for plasma display panels [15]. The glass transition temperature ($T_g$ = 480–560 °C), thermal expansion coefficient (7–9 × $10^{-6}$/°C) and dielectric constant (ε = 14–19) for bulk glass have been reported [16]. Kim et al. evaluated the effect of coordination number on glass properties [17]. But this glass has not yet been explored for advanced capacitors, in which the interest is the behavior of the material near the melting temperature to achieve viscous flow/liquid phase sintering. As indicated by the differential thermal analysis (DTA) curves, although not mentioned in [16], the phases in the high temperature range are quite complicated and the crystallization/melting temperatures depend on the glass composition as well as the particle size. The behavior of BaO–$B_2O_3$–ZnO near the melting temperature needs to be clarified before this glass is used to fabricate the advanced capacitors to store energy. In this work, we investigate the change of the phases, composition, microstructure, and properties of BaO–$B_2O_3$–ZnO films prepared by pulsed laser deposition (PLD), with the heat-treatment, as well as the effect of heat-treatment on the capacitance of the fabricated capacitor. Our final goal is to find the optimal process to make high performance capacitors via viscous flow/liquid phase sintering.

## 2. Experimental

30 BaO–45 $B_2O_3$–25 ZnO (mol%) glass target was prepared by melting the mixture of the reagent grade chemicals, barium carbonate ($BaCO_3$), boron oxide ($B_2O_3$), and zinc oxide (ZnO). In order to simulate the process to produce high performance capacitors via viscous flow/liquid phase sintering, the films were prepared by PLD [18] and heat-treated at various temperatures. KrF pulsed laser (wavelength 248 nm, pulse width 30 ns) was used as the excitation source for the deposition. The laser beam size is ~1.35 × 4.14 $mm^2$ with the energy of ~100 mJ. The working pressure is 0.3 mTorr Ar. The heavily doped n-type Si (100) wafer (0.001–0.006 Ω cm) was used to reduce the contribution of substrate capacitance to the total capacitance. After deposition, the wafer was broken into small pieces of samples, which were heat-treated at various temperatures for 45 min and then cooled in the furnace to room temperature with the protection of Ar to avoid formation of thicker $SiO_2$ on the substrate backside. After heat-treatment, the substrate backside oxide was removed by plasma-therm etching with the gas mixture of $CHF_3$ and $O_2$ (~9:1) at the pressure of 0.03 Torr. The oxide removal is confirmed by using thermal $SiO_2$ sample as a reference. The capacitor stack was then formed by depositing Ti/Al contact electrode on both sides in the radio frequency sputtering system. Before making the contact electrode on the backside, the Si substrate backside was *in-situ* cleaned in the sputtering system in order to make sure the oxide was removed completely and then form the ohmic contact. DTA of BaO–$B_2O_3$–ZnO powder was carried out in the range of 200 to 1000 °C with heating rate of 10 °C/min under a Helium flow of 50 mL/min on a NETZSCH STA 409C/CD equipment using $Al_2O_3$ as a reference. X-ray photoelectron spectroscopy (XPS) characterization was performed in a PHI 5000 Versa probe, ΦnULVAC-PHI, Inc., Scanning ESCA Microscope using monochromatic Al $K_\alpha$ X-rays (1486.6 eV) at a base pressure of ~$10^{-10}$ Torr. Sputtering cleaning of the sample surface was achieved via the energized Ar+ bombardment. The capacitance was measured on a HP 4192A impedance analyzer with the frequency of 5 Hz–13 MHz (HEWLETT-PACKARD). Scanning electron microscope (SEM) images were taken on the machine of Carl Zeiss Supra SEM. X-ray diffraction (XRD) patterns were collected using an X-ray diffractometer (PANalytical, X'pert Pro.) with Cu $K_\alpha$ radiation (λ = 1.5406 Å) generated under the applied voltage of 40 keV and the current of 25 mA.

## 3. Results

Glass transition temperature ($T_g$) and crystallization temperature ($T_b$) of the BaO–$B_2O_3$–ZnO glass are identified to be 536 °C and 640 °C, respectively, from the change and the peak of the DTA curve shown in Fig. 1. As indicated by three troughs in the DTA curve, BaO–$B_2O_3$–ZnO glass goes through three melting transitions in the range of 700 °C to 900 °C, occurring at 766 °C, 810 °C, and 866 °C, respectively. Fig. 2 shows SEM images for the films after heat-treatment at different temperatures. As shown in Fig. 2(a), the as-deposited film has a quite high porosity and consists of the particles with different morphologies: sphere, drop-like particles, dog-bone, and flat-pellet, and so on. The variable morphology of the particles is a characteristic feature of PLD process. In PLD, laser radiation energy is converted first into electronic excitation and then into thermal, chemical, and even mechanical energy to cause evaporation, ablation, excitation, plasma formation, and exfoliation. Constituents of the "plume" consist of a mixture of energetic species including atoms, molecules, electrons, ions, clusters, micro-sized solid particulates, and molten globules [18]. Therefore, a mixture of these species is included in the deposited film which shows the complex microstructure such as the one shown in Fig. 2(a). Some particles are covered by the very small particles (several nanometers) and form the cactus-like spheres, as shown in Fig. 2(d). It is this unique characteristic of PLD that offers us the opportunity to simulate the real film made of particles which can be available from methods such as mechanical milling. The film has no microstructural change after 500 °C heat-treatment, as shown in Fig. 2(b). But the microstructural change can be observed for the film heat-treated at 600 °C, as shown in Fig. 2(c), because the heat-treatment temperature is higher than the glass transition temperature (536 °C). For instance, the particle surface becomes smooth and the particles begin to fuse together. But the porosity of the film is still quite high. However, a greater difference can be observed for the film heat-treated at 700 °C. The particles are now almost completely joined in the film which is becoming continuous and denser, as shown in Fig. 2(e). It can be seen that the particles have no crystallographic morphology, i.e., the particle surface is very smooth and round. This indicates that the particles still possess the amorphous phase. Combined with bulk crystallization temperature (640 °C) and XRD pattern discussed in a later section, the film heat-treated at 700 °C is a composite consisting of crystalline and amorphous phases. After the film heat-treated at 800 °C, as shown in Fig. 2(f) and (g), the particles are showing crystallographic morphology, i.e., the sharp edges and the flat surfaces, indicating that the particles are crystalline (granular). The additional evidence for the major crystalline phase is provided by SEM cross-section image of this film which shows the lamellar layers

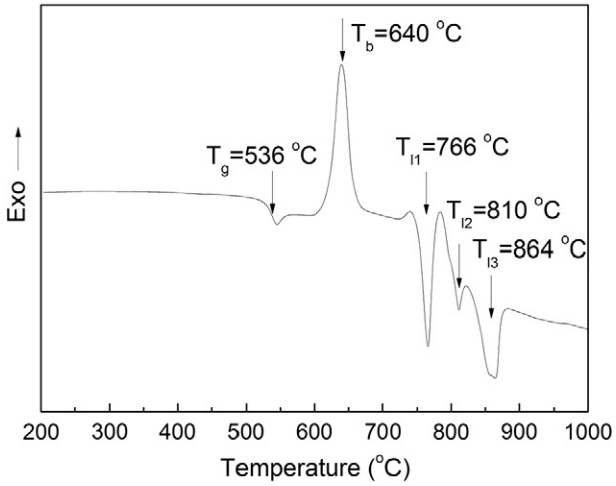


**Fig. 1.** DTA curve of 30 BaO–45 $B_2O_3$–25 ZnO glass powder (mol%).

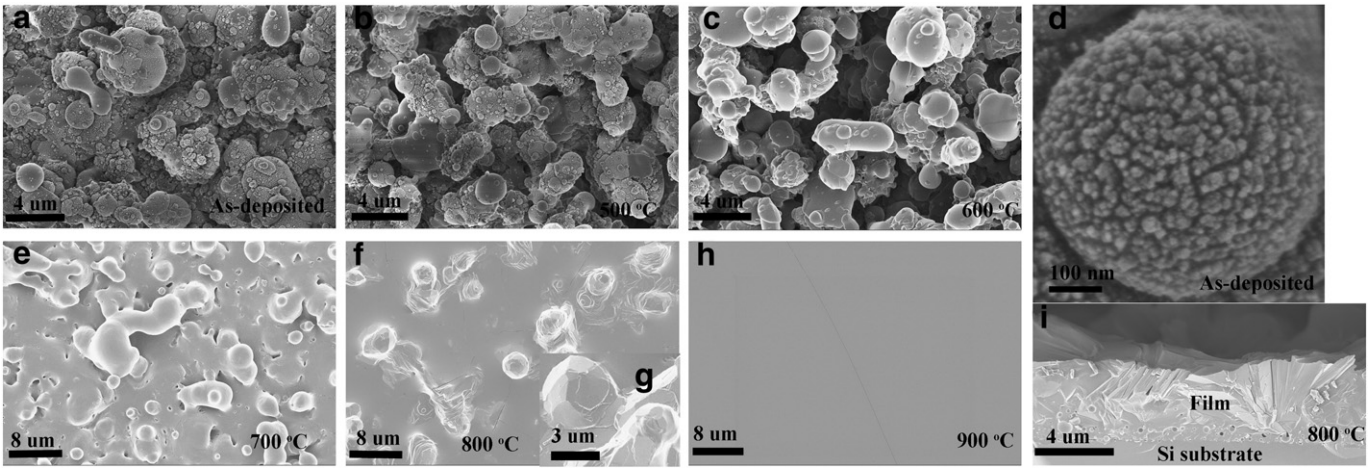


**Fig. 2.** SEM images of the $BaO–B_2O_3–ZnO$ films. (a)–(h) are the topdown images for the films as deposited and heat-treated at various temperatures. (a) and (d) as-deposited, (b) heat-treated at 500 °C, (c) heat-treated at 600 °C, (e) heat-treated at 700 °C, (f) and (g) heat-treated at 800 °C, (h) heat-treated at 900 °C, (i) is the cross-section image for the film heat-treated at 800 °C. The heat-treatment time was 45 min.

in the particles, as shown in Fig. 2(i), and the lamellar domains in the matrix which becomes flat since the film went through the melting of a crystalline phase (766 °C). It can be seen from Fig. 2(h), after the film heat-treated at 900 °C, that the film surface becomes very flat and shows very large grain size. Compared with the film heat-treated at 800 °C, the flat surface of the film indicates that the crystalline particles were melted during the heat-treatment (900 °C) and then formed the new film with the matrix. The flat interface between the substrate and the film can be clearly seen. Around the interface there are lots of voids which cannot be observed for the films heat-treated at 700 °C and 900 °C.

Fig. 3 shows the capacitance of capacitors made from the films heat-treated at 700 °C to 900 °C. The inset shows the schematic structure configuration of the capacitor. The thickness is 3.4 μm, 3.6 μm and 2.6 μm, respectively, for the films heat-treated at 700 °C, 800 °C, and 900 °C. The thickness variation at lower temperatures is believed to be from the non-uniformity of PLD films. The device area is 1 $mm^2$. Although the as-deposited film and the films heat-treated below 600 °C were used to make the capacitors, since these films have a very rough surface and high porosity (see Fig. 2), the obtained data for the capacitors made by using these films are not reliable and not shown here. As shown in Fig. 3, the capacitance of the heat-treated film decreases with the heat-treatment temperature. The film after low temperature heat-treatment (700 °C) has a high dielectric constant that is close to the dielectric constant (ε = 14–19) of bulk glass [16].

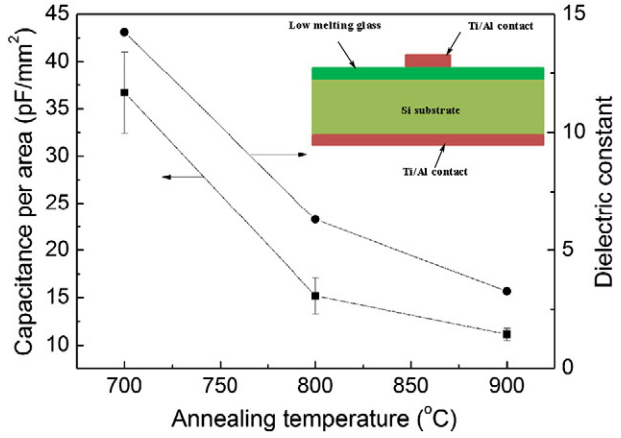


**Fig. 3.** The effect of heat treatment temperature on the capacitor capacitance and the film dielectric constant. The inset shows the schematic configuration of the capacitor.

Therefore, the optimal temperature to make the capacitor is 700 °C, at which the particle-like film is sintered. Since the liquidus surfaces of the $BaO–ZnO–B_2O_3$ ternary system change with the composition in the system [19], further tuning of the optimal sintering temperature is possible. The reason for the reduction of dielectric constant with the heat-treatment temperature is not clear. It may be caused by the crystallization and the phase change of the film, the reduction of Zn concentration, the diffusion of Si into the film, the growth of $SiO_2$ at the interface between the film and the substrate, and the voids in the films near the substrate–film interface. The capacitance has only a little dependence on the frequency as well as on the temperature for the capacitors made from the film heat-treated at both 700 °C and 900 °C. Even at high frequency of 10 MHz, for the capacitors made from the film heat-treated at 700 °C, the capacitance remains unchanged. This is in agreement with the report in reference [16], where the dielectric constant does not change with the frequency.

## 4. Discussion

As indicated by the DTA curve in Fig. 1 and DTA curves in Kim et al.'s paper [16], the $BaO–B_2O_3–ZnO$ glass goes through several transitions such as the solid–liquid transition and the solid–solid transition. Sato [19] determined the liquidus surface and the isothermal section at 500 °C of the pseudo-ternary $BaO–ZnO–B_2O_3$ system by the thermal analysis and X-ray diffraction. In his study, there are three phase transformations near the composition studied in this paper. They are one ternary eutectic reaction, and two peritectic reactions. The ternary eutectic reaction occurs at 765 ± 10 °C with the composition of 34 mol% BaO–21 mol% ZnO–45 mol% $B_2O_3$ by the equation: $L \rightarrow BaO.B_2O_3 + ZnO.B_2O_3 + 5ZnO.2B_2O_3$. The peritectic reactions take place at 782 ± 10 °C and ~870 °C. These three reaction temperatures match the temperatures of the three troughs observed on DTA curve shown in Fig. 1. Therefore, from 500 to 900 °C heat treatment, the $BaO–B_2O_3–ZnO$ went through one ternary eutectic reaction at 765 °C and then the peritectic reactions at higher temperatures. Lamellar structures were observed in glass-crystal structures by progressive solidification of the eutectic in the system $ZnO–B_2O_3$. The laminate was composed of alternate laths of single crystal $5ZnO.2B_2O_3$ and vitreous $ZnO.B_2O_3$. Due to intrinsic solidification characteristic of the eutectic, the laminar structures observed in this study also could be from the ternary eutectic reaction mentioned above. The indirect evidence is that this laminar structure is not observed for the sample heat-treated at 700 °C but observed only for the film heat-treated at 800 °C which is slightly higher than the ternary eutectic reaction temperature of ~766 °C.

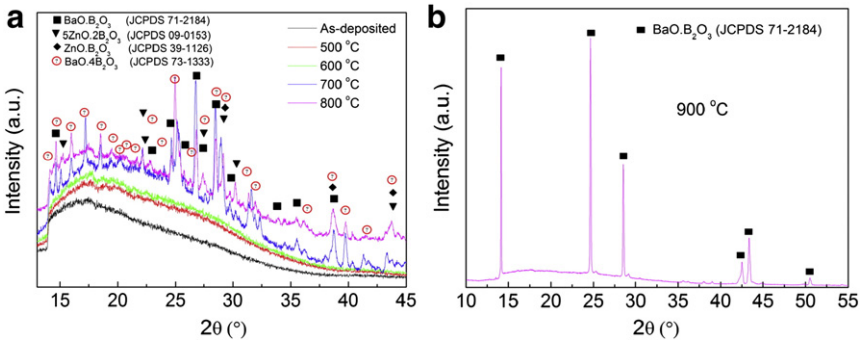


**Fig. 4.** XRD patterns of the deposited film and the films heat-treated at various temperatures. (a) As-deposited film and the films heat-treated at 500 °C to 800 °C, (b) the film heat-treated at 900 °C. The heat-treatment time was 45 min.

The three equilibrium phases are $BaO.B_2O_3$, $5ZnO.2B_2O_3$, and $ZnO.B_2O_3$, based on the phase equilibrium diagram for the composition studied in this work. In the neighboring regions, the equilibrium phases are $BaO.2B_2O_3$, $BaO.B_2O_3$, $ZnO.B_2O_3$ and $BaO.B_2O_3$, $5ZnO.2B_2O_3$, ZnO, respectively. More details are described in [19]. As pointed out by Sato [19], the liquidus lines and the eutectic points in the pseudo-binary sections, for which only a small number of experimental points were available, were determined by extrapolating the liquidus lines connecting measured points into the other pseudo-binary sections so that no inconsistency might occur in the ternary phase diagram. Therefore, it is possible that all phases ($BaO.B_2O_3$, $5ZnO.2B_2O_3$, $ZnO.B_2O_3$, $BaO.2B_2O_3$ and ZnO) could exist in the crystallized films. Fig. 4 shows the XRD patterns for the as-deposited film and the films heat-treated at 500 °C, 600 °C, 700 °C, 800 °C, and 900 °C. As indicated by the single broad peak in Fig. 4(a), the as-deposited film and the films heat-treated below 600 °C are amorphous. But the films show sharp XRD peaks after heat-treatment above 700 °C. Comparing XRD patterns for the films heat-treated at 700 °C, 800 °C, and 900 °C (Fig. 4(b)), these films show different peaks, especially the film heat-treated at 900 °C, which shows only a few very strong peaks. This indicates that the films heat-treated from 700 °C to 900 °C have different phases and may have mixed phases as predicted above. Let us analyze the phases starting from the simple case. As shown in Fig. 4(b), a few very strong peaks observed for the film heat-treated at 900 °C indicate that the phases in this film could be dominated by a single phase or this heat-treated film only has a single phase. After searching all possible phases, the best matching JCPDS is 71-2184 for rhombohedral barium borate ($BaB_2O_4$ or $BaO.B_2O_3$). But compared with the powder diffraction of $BaO.B_2O_3$, the high c index planes do not show up. For example, the strongest peak for barium borate is (1 0 10) which is not shown in the heat-treated film, but the strongest peak for the film heat-treated at 900 °C is (1 1 0) peak, which indicates that the heat-treated film has the preferential texture. As indicated by many sharp peaks in Fig. 4(a), the phases in the films heat-treated at 700 °C and 800 °C are quite complicated. It can be seen that XRD intensity at 36° (2θ), which is located by the strongest peak of ZnO, for both the films heat-treated at 700 °C and 800 °C is quite weak. So the possibility to have ZnO in the film is quite low or the amount of ZnO is very small if any. Comparing the reported crystal structures with the XRD patterns plus the phases predicted in [19], the phases in the films heat-treated at 700 °C and 800 °C consist of rhombohedral $BaO.B_2O_3$ (JCPDS 71-2184), β-$5ZnO.2B_2O_3$ (JCPDS 09-0153), cubic $ZnO.B_2O_3$ (JCPDS 39-1126), and monoclinic $BaO.2B_2O_3$ (JCPDS 73-1333). Due to phase complication, other phases could be indentified from the XRD pattern by combining these phases. For example, $Ba_2Zn(B_3O_6)_2$ (JCPDS 85-0294) could be considered as the combination of $BaO.B_2O_3$ and $ZnO.B_2O_3$. Besides the inconsistent prediction from the limited experimental data in [19], the existence of $BaO.2B_2O_3$ could also be caused by Zn concentration reduction in the heat-treated films which will be discussed later. It can be seen that there are some XRD pattern differences between the films heat-treated at 700 °C and 800 °C. These differences could be from the phase ratio differences in the film and the composition differences in the phases. It should be noted that the phases in the film heat-treated at 700 °C are formed by solid–solid transition, that is, heat treatment of the glass film caused the vitreous phase to devitrify into the different phases crystallites. However, the phase transformation for the film heat-treated at 800 °C is via liquid–solid transition. The scenario can clearly be explained by the differences in crystallographic morphology in these two films, as shown in Fig. 2(e) and (f). Table 1 summarizes the phases and the dielectric constant for the films heat-treated at different temperatures.

Fig. 5(a) shows the XPS spectra of Zn $2p^3$ core level for the films heat-treated at 700 °C, 800 °C and 900 °C with or without surface sputtering cleaning. It can be clearly seen that the intensity of Zn $2p^3$ decreases with the heat-treatment temperature,independent of surface sputtering cleaning. Especially for the film heat-treated at 900 °C without surface sputtering cleaning, the Zn signal is almost at noise level. After surface sputtering cleaning, the weak peak can be observed with the center of ~1020 eV. The observed asymmetry of Zn $2p^3$ peaks for the film after surface sputtering could be caused by the different chemical states inside the films. This asymmetry characteristic has been observed for aluminum-doped ZnO films [20]. Different from the case for the film heat-treated at 900 °C, after surface sputtering cleaning, the intensity of Zn signal is reduced for the film heat-treated at 700 °C and 800 °C. Therefore, Zn is richer on the surface than inside for the films heat-treated at 700 °C and 800 °C but poorer than inside for the film heat-treated at 900 °C. This could provide the information that Zn diffuses onto film surface and evaporates away at 900 °C. It can also be seen that the peak shifts from 1021.8 eV to 1020.4 eV for the film heat-treated at 700 °C and 800 °C after surface sputtering cleaning. It is reported that the binding energy of Zn $2p^3$ is around 1022 eV for Zn – O bond in ZnO. Therefore, on the surface the chemical state of Zn is like the one in ZnO. Shown in Fig. 4 in [21], the evaporation of ZnO begins after 600 °C and then rapidly increases after 800 °C. As shown in Fig. 5(b), the Zn concentration in the film decreases when the heat-treatment temperature is higher than 600 °C. Therefore, Zn

**Table 1**
The crystallization and dielectric constant of the films heat-treated at different temperatures.

| Temperature (°C) | Film crystallization (phases) | Dielectric constant |
|---|---|---|
| <600 | Amorphous | 14–16 [16] |
| 700 | Partial crystallization ($BaO.B_2O_3$, $5ZnO.2B_2O_3$, $ZnO.B_2O_3$, $BaO.2B_2O_3$) | 14.3 |
| 800 | Partial crystallization ($BaO.B_2O_3$, $5ZnO.2B_2O_3$, $ZnO.B_2O_3$, $BaO.2B_2O_3$) | 6.3 |
| 900 | Full crystallization ($BaO.B_2O_3$) | 3.3 |

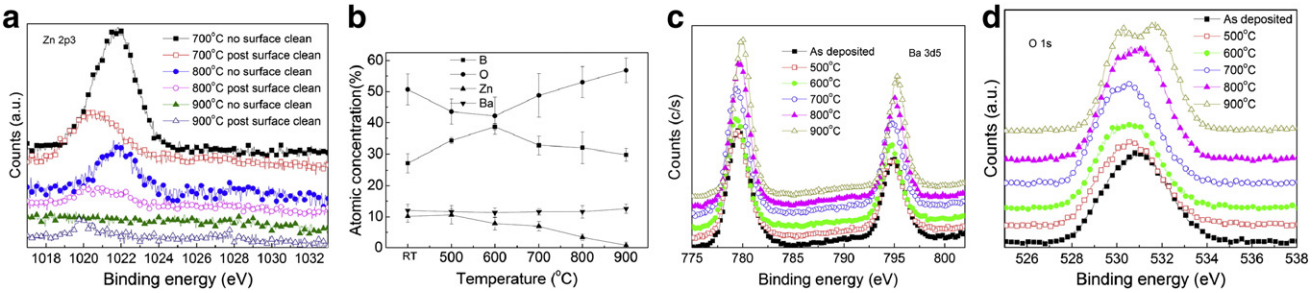


**Fig. 5.** The XPS data for the as-deposited film and the films heat-treated at various temperatures. (a) Zn $2p^3$ spectra with/without surface sputtering, (b) atomic concentrations, (c) Ba $3d^3/3d^5$ spectra and (d) O 1s spectra without surface sputtering.

significant reduction could be caused by the evaporation on the surface when the film is heat-treated at temperature higher than 800 °C. This also provides an explanation why the film gives the XRD pattern similar to that of $BaO.B_2O_3$ at 900 °C, since it is well-known that barium borate ($BaO.\ B_2O_3$) has the dielectric constant of 6.7–8.1. Therefore, the reduction of Zn concentration could be one of the reasons to reduce the dielectric constant of the film. In addition, from Fig. 5(c), the peaks of Ba $3d^3/3d^5$ spectra are centered at 779.6 eV and 795.3 eV for the as-deposited film, respectively. With the increasing heat-treatment temperature, these two peaks shift to higher binding energy, especially for the heat-treatment temperature higher than 700 °C. For instance, the peaks of Ba $3d^3/3d^5$ spectra for the film heat-treated at 900 °C are located at 779.9 eV, and 795.6 eV, respectively. These peaks have 0.3 eV shift to higher binding energy from those of the as-deposited film. Similar shift is observed for B 1 s spectra. The shift of the binding energy to higher energy indicates that the crystallization of the material makes the $Ba^{2+}$ and $B^{+}$ ions more positive, probably due to the shorter atom distance in crystalline material than that in the amorphous material and the Zn concentration reduction. It should be noted that Si signal is also observed in the XPS survey for the film heat-treated at 900 °C, indicating that the Si could diffuse into the film from the substrate at this temperature. Fig. 5(d) shows the high resolution XPS spectra of O 1s core level for the films. Instead of single peak as observed for the film heat-treated lower than 800 °C, the spectra of O 1s core level for the film heat-treated at 900 °C is split into two peaks with the center of 530.4 eV and 531.7 eV. The former is from the O bond in the film and the latter could be from Si – O bond. Si diffusion into the film could also contribute to the dielectric constant reduction of the film heat-treated at higher temperature. This could be the reason that the dielectric constant is too low for the film heat-treated at 900 °C. Further investigation is needed.

## 5. Conclusion

Changes of microstructures, phases, and properties of $BaO–B_2O_3–ZnO$ films as a function of heat-treatment were investigated. The film heat-treated at 700 °C became continuous and denser and its porosity was greatly reduced. Heat-treatment at 800 °C and 900 °C caused the significant microstructure changes of the films due to ternary eutectic reaction at 766 °C and the peritectic reaction at 864 °C. The phases in the films heat-treated at 700 °C and 800 °C are quite complicated, but the film heat-treated at 900 °C is dominated by a single phase. Zn reduction, Si diffusion, and crystallization could be the reasons to reduce the dielectric constant of the film. The capacitor made by the film heat-treated at 700 °C shows the highest capacitance and highest dielectric constant which indicates the optimal temperature to use the low melting glass $BaO–B_2O_3–ZnO$ to make the high performance capacitor by viscous flow/liquid phase sintering is around 700 °C.

## Acknowledgment

This work was supported by the U.S. National Science Foundation under the Emerging Frontiers for Research and Innovation, NSF-EFRI Grant 1038272 Program (for renewable energy storage), overseen by the NSF Engineering Directorate.

## References

[1] A.S. Arico, P. Bruce, B. Scrosati, J.M. Tarascon, W. van Schalkwijk, Nanostructured materials for advanced energy conversion and storage devices, Nat. Mater. 4 (2005) 366–377.
[2] S. Jennifer, A heroic capacity: can capacitors save the world's energy and transportation systems? Am. Ceram. Soc. Bull. 88 (2009) 19–25.
[3] D. Chrisey, Nanostructured Capacitors for Renewable Energy Storage, SPIE Newsroom, 2011. 1–2.
[4] M.J. Pan, C.A. Randall, A brief introduction to ceramic capacitors, IEEE Electr. Insul. Mag. 26 (2010) 44–50.
[5] J. Ihlefeld, B. Laughlin, A. Hunt-Lowery, W. Borland, A. Kingon, J.P. Maria, Copper compatible barium titanate thin films for embedded passives, J. Electroceram. 14 (2005) 95–102.
[6] J.M. Haussonne, G. Desgardin, P.H. Bajolet, B. Raveau, Barium titanate perovskite sintered with lithium fluoride, J. Am. Ceram. Soc. 66 (1983) 801–807.
[7] N.J. Smith, B. Rangarajan, M.T. Lanagan, C.G. Pantano, Alkali-free glass as a high energy density dielectric material, Mater. Lett. 63 (2009) 1245–1248.
[8] C.T. Cheng, M. Lanagan, B. Jones, J.T. Lin, M.J. Pan, Crystallization kinetics and phase development of $PbO–BaO–SrO–Nb_2O_5–B_2O_3–SiO_2$-based glass-ceramics, J. Am. Ceram. Soc. 88 (2005) 3037–3042.
[9] E. Gorzkowski, M.J. Pan, B. Bender, C. Wu, Glass-ceramics of barium strontium titanate for high energy density capacitors, J. Electroceram. 18 (2007) 269–276.
[10] R.G.P. McQuaid, L.J. McGilly, P. Sharma, A. Gruverman, J.M. Gregg, Mesoscale flux-closure domain formation in single-crystal $BaTiO_3$, Nat. Commun. 2 (2011) 404.
[11] L. Wu, M.C. Chure, K.K. Wu, W.C. Chang, M.J. Yang, W.K. Liu, M.J. Wu, Dielectric properties of barium titanate ceramics with different materials powder size, Ceram. Int. 35 (2009) 957–960.
[12] H. Watanabe, H. Oshita, M. Ohji, K. Hadano, Dielectric forming material for use in plasma display panel and glass powder used therefor, 2000. US Patent 6010973.
[13] S. Fujimine, S. Ootaki, T. Manabe, K. Yamanaka, M. Tanida, Y. Aoki, Low melting point glass for covering electrodes, and glass ceramic composition for covering electrodes, , 2002. , US Patent 6376400.
[14] M. Tanida, T. Fukahori, Glass for covering electrodes and plasma display panel, 2010. US Patent 7749929.
[15] H. Masuda, R. Kimura, N. Sakamoto, K. Morinaga, Properties and structure of glasses in the system $BaO–B_2O_3–ZnO$, J. Jpn. Inst. Met. 63 (1999) 284–288.
[16] D.N. Kim, J.Y. Lee, J.S. Huh, H.S. Kim, Thermal and electrical properties of $BaO–B_2O_3–ZnO$ glasses, J. Non-Cryst. Solids 306 (2002) 70–75.
[17] Y.S. Kim, Y.J. Jung, K.H. Lee, T.H. Kim, B.K. Ryu, Properties and structure of $BaO–ZnO–B_2O_3$ glasses, Key Eng. Mater. 368–372 (2008) 1433–1435.
[18] D.B. Chrisey, G.K. Hubler, Pulsed Laser Deposition of Thin Films, John Wiley & Sons, New York, New York, 1994.
[19] H. Sato, Liquidus surfaces and isothermal section at 973 K of the $BaO–ZnO–B_2O_3$ pseudo-ternary system, Mater. Trans. 47 (2006) 2910–2917.
[20] M.N. Islam, T.B. Ghosh, K.L. Chopra, H.N. Acharya, XPS and X-ray diffraction studies of aluminum-doped zinc oxide transparent conducting films, Thin Solid Films 280 (1996) 20–25.
[21] F.E. Dart, Evaporation of zinc and zinc oxide under electron bombardment, Phys. Rev. 78 (1950) 761–764.